Welding in the World
https://doi.org/10.1007/s40194-025-01971-1

RESEARCH PAPER

A streamlined FE method for deformation and residual stress prediction in butt welding using continuous heat input

Xiaoyu Guan[1] · Mikihito Hirohata[1] · Kyong-Ho Chang[2]

Received: 23 September 2024 / Accepted: 3 February 2025

Abstract
Finite element (FE) analysis is useful to estimate and predict deformation and residual stress generated by welding. To improve the efficiency of the FE analysis for the welding process, this study proposed an element combination and heat input method for simulating the butt welding process on steel with a V-shaped groove. This method integrated shell and solid elements and input heat energy continuously into the weld metal elements considering the energy distribution. Additionally, a parametric study of the double ellipsoidal model was conducted within the Continuous Distributed (CD) heat input method to identify optimal parameters for accurately simulating the heat source. The simulation results of the models using different heat input methods of deformation and residual stress were in good agreement with the experimental results, and the model using the continuously distributed heat input method saved 54% computational time compared to that by a conventional heat input method without considering the energy distribution. It was indicated that the proposed method for simulating the butt welding process was effective and could significantly reduce computational time.

Keywords Finite element method · Butt welding · Heat input model · Temperature histories · Out-of-plane deformation · Residual stress

1 Introduction

Welding is a critical technique in the fabrication of steel structures, providing strong and reliable joints that are essential for a wide range of engineering applications. As a highly effective method, welding offers a lightweight solution for the construction of steel structural components, thereby enhancing both the efficiency and the structural integrity of the resulting assemblies. However, during the welding process, the generation of welding deformation and residual stress is inevitable. Welding deformation significantly impacts the precision of assembly, the aesthetic quality, and the mechanical integrity of welded structures. The presence of such deformations necessitates corrective measures, which consequently incur additional costs and contribute to delays in the overall project timeline [1]. The welding process inherently induces residual stresses within the welded components, which can significantly affect the structural integrity. These residual stresses, particularly in regions near the weld beads, can lead to detrimental phenomena such as brittle fractures, fatigue failures, and stress corrosion cracking [2, 3]. Therefore, understanding and mitigating the effects of welding-induced residual stresses are critical for ensuring the longevity and safety of welded structures [4–6].

Finite element method (FEM) has emerged as a powerful and versatile tool for simulating the entire fabrication process of the joints to precisely assess and forecast the deformation and residual stresses caused by welding. Numerous studies have utilized FEM to achieve this goal [7–9]. Liu et al. [10] explored the impact of constraints on the welding process in thin-walled stainless steel pipes using both experimental methods and numerical simulations. Their

Recommended for publication by Commission XV - Design, Analysis, and Fabrication of Welded Structures

✉ Mikihito Hirohata
hirohata@civil.eng.osaka-u.ac.jp

Xiaoyu Guan
x-guan@civil.eng.osaka-u.ac.jp

Kyong-Ho Chang
changkor@cau.ac.kr

[1] Graduate School of Engineering, Osaka University, Osaka 565-0871, Japan

[2] Department of Civil Environment & Plant Engineering, Chung-Ang University, Seoul 06974, South Korea

Published online: 19 February 2025

study demonstrated that incorporating the clamping effect into the welding simulation revealed that decreasing the constraint distance is the most effective strategy for minimizing welding distortion in seam-welded pipes. Similarly, Zhang et al. [11] devised a three-dimensional thermomechanical coupling method to forecast the residual stress distribution in multi-pass welded joints. Using this computational technique, they calculated the residual stress distributions in column-beam welded structures, butt-welded joints under structural restraint, and in a free state. The findings indicate that structural restraints and neighboring welded joints within the structure markedly influence the residual stress distribution.

Different welding techniques require unique approaches to predict and control residual stress and deformation due to their distinct thermal and mechanical characteristics. For example, Das et al. utilized a Coupled Eulerian and Lagrangian (CEL) approach combined with a physics-informed machine learning model to optimize residual stress in dissimilar friction stir welding, showcasing the potential of advanced modeling for solid-state welding [12]. In fusion welding, De and DebRoy highlighted the influence of heat input and material properties on residual stress, proposing a thermo-elasto-plastic finite element framework to address these effects [13]. Mahmood et al. investigated residual stress and thermal behavior in wire arc-based welding and additive manufacturing by integrating analytical and finite element models, demonstrating the effectiveness of hybrid modeling techniques [14]. Furthermore, Huang et al. explored a hybrid gouging and welding process, revealing the evolution of residual stress and deformation through experimental and numerical studies [15]. Despite the benefits of FEM, a comprehensive framework that unifies modeling across diverse welding processes remains an ongoing challenge. And welding also continues to present a challenging thermo-mechanical coupling phenomenon. The material's mechanical properties alter dynamically with temperature, introducing additional layers of complexity to the simulation process. These factors contribute to the inherent instability and convergence difficulties in calculations, particularly when contrasted with simulations of purely mechanical phenomena. As a result, welding simulations typically demand substantial time and computational resources for accurate modeling and computation.

To reduce modeling and computation time, various researchers have identified methods that markedly enhance simulation efficiency. Murakawa et al. [16] shortened computation time by applying the iterative substructure method (ISM). In this method, the highly non-linear region near the local weld zone was iteratively treated as a substructure. The displacement at the boundary between the substructure and the remaining area, modeled as linear elasticity, was calculated using the entire finite element model. This displacement then served as the boundary condition for solving the substructure, and iterative corrections were made by accounting for the unbalanced forces at the boundary. Ikushima et al. [17] introduced the idealized explicit finite element method (IEFEM) to reduce computational time and minimize memory usage. Furthermore, this IEFEM is optimized for parallel processing through a Graphics Processing Unit (GPU). Although these techniques significantly boost simulation efficiency, their versatility remains a concern. It is essential to investigate whether these methods can be applied universally to all welding scenarios. Additionally, exploring other effective approaches to enhance simulation efficiency is necessary.

Among various simplification techniques for welding simulation, the authors explored using shell elements to partially or fully replace solid elements, thus reducing the size of the stiffness equation to be solved. Previous studies have proposed simplified modeling approaches for T-shaped joints using shell elements [18, 19]. These approaches demonstrated that substituting solid elements with shell elements, either partially or completely, can significantly decrease computation time. Notably, partial replacement of solid elements with shell elements can preserve the model's accuracy. However, further research is needed to validate this method's applicability to other types of welded joints and to expand its effectiveness.

To verify the method's applicability and enhance calculation efficiency by refining the heat source model, this study developed an integrated shell-solid element model. It systematically investigated the effects of various heat input methods in the heat source model on the simulation results of butt-welded joints [20]. The research aims to deepen the understanding of heat input mechanisms in simulations and to establish a comprehensive set of simulation methodologies. These methodologies should accurately reproduce the intricate details of the welding process while significantly reducing computation time. By focusing on the heat input aspect, the proposed approach is inherently adaptable to different welding techniques, making it versatile across various processes such as friction stir welding, fusion welding, and hybrid welding methods. Ultimately, the goal is to improve predictive capabilities regarding deformation and residual stress in butt-welded joints, thus contributing valuable insights and tools for engineering applications. This study aspires to provide practical solutions that enhance the reliability and efficiency of welded structures in real-world scenarios. For ease of reading, all abbreviations and symbols used in the following section are detailed in the Appendix.

2 Experiment

2.1 Specimen

A steel plate with a groove in the middle was used to fabricate a three-pass butt-welded joint. The welding method was gas metal arc welding. The shape of the specimen is

shown in Fig. 1. The specimen had a width of 500 mm and a thickness of 12 mm. Regarding its length, the two edge sections were 300 mm each, while the central area was 380 mm long and 50 mm wide. The V-shaped groove, located within the central area, had a length of 340 mm, a root face of 1 mm, and an opening angle of 50°. The number of specimens was two. The materials of the plate and weld metal were general structural steel of SM400A and YGW11 prescribed by JIS G3106 and JIS Z3312, respectively. The mechanical properties and chemical compositions of the materials are shown in Table 1.

2.2 Experimental procedure

Prior to butt welding, the internal stresses within the plates were alleviated through annealing. The welding parameters are shown in Table 2. To monitor the temperature variations, four thermocouples were affixed to the top surface of the plate, with their locations indicated in Fig. 1. Out-of-plane deformations were measured along the midspan in the y direction ($x=0$ mm, $y=\pm30,\pm65,\pm105,\pm155,\pm235,\pm250$ mm), as indicated by the green line in Fig. 1, using a dial gauge. The edge points were used as reference locations, and deformation differences at other positions were calculated by comparing measurements taken before and after welding. Residual stresses in the y direction ($x=-30$ mm) were assessed using X-ray diffraction (XRD; μ-X360s, Pulstec Industrial Co., Ltd.), with the measurement locations indicated by the orange line in Fig. 1. Stress measurements were performed in both the x and y directions. In the region near the weld bead, residual stresses were measured at $y=\pm9,\pm12,\pm15,\pm18,\pm21$ mm, with measurements taken at 3-mm intervals. For the region farther from the weld bead, measurements were conducted at $y=\pm26,\pm31,\pm36,\pm41,\pm46,\pm51,\pm56$ mm, with 5-mm intervals. These regions were selected to capture the gradient of residual stresses transitioning from areas close to the weld bead to those farther away.

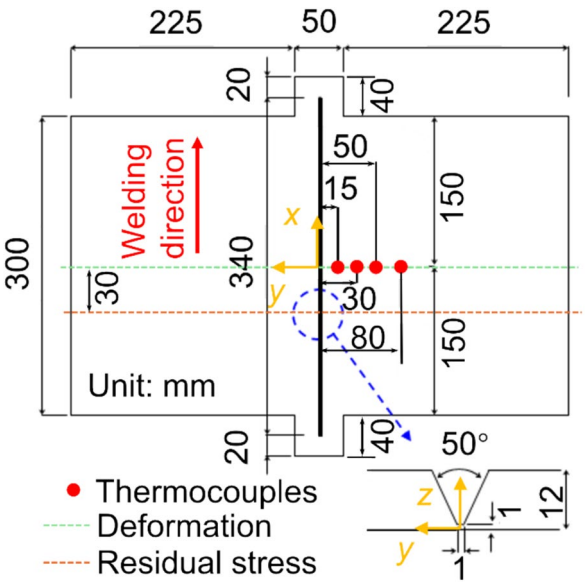

Fig. 1 Shape and dimension of the specimen

3 Numerical simulation

3.1 Thermal and elastoplastic analysis

In this section, a thermal–mechanical coupled numerical simulation model was applied to simulate the butt welding process. In the thermal analysis, assuming Fourier's law for heat flux and the absence of melt flow during solidification [9, 21], the energy balance for each subdomain Ω_i follows the classical energy balance Eq. (1):

$$\rho\frac{\partial\mathcal{H}}{\partial t}-\nabla\bullet(\kappa\nabla T)=q\ \forall(\boldsymbol{x},t)\in\Omega_i \tag{1}$$

In elastoplastic analysis, the total strain comprises contributions from elastic, plastic, thermal strains, and strains due to solid-state phase transformations [9]. For low carbon steel, since the influence of phase transformations on deformation and residual stress caused by welding is minimal, the total strain rate can be expressed by Eq. (2):

Table 2 Welding conditions of each pass

	Current	Voltage	Speed
Pass	A	V	mm/s
1	120	20	5.2
2	115	20	2.8
3	105	20	2.1

Table 1 Mechanical properties and chemical compositions of materials

	Mechanical properties			Chemical compositions				
	Yield stress	Ultimate strength	Elongation	C	Si	Mn	P	S
	N/mm^2	N/mm^2	%	wt%				
Base metal	304	455	30	0.16	0.20	0.53	0.026	0.005
Welding wire (Catalogue value)	490	570	31	0.08	0.51	1.10	0.010	0.010

$$\dot{\varepsilon} = \dot{\varepsilon}^{e} + \dot{\varepsilon}^{p} + \dot{\varepsilon}^{th} \tag{2}$$

The elastic behavior is typically characterized by a hypoelastic relation, as presented in Eq. (3):

$$\hat{\sigma}_{GN} = E^{e}\dot{\varepsilon}^{e} + \frac{dE^{e}}{dT}\dot{T}\varepsilon^{e} \tag{3}$$

The elastic strain behavior is characterized by isotropic Hooke's law, incorporating a temperature-dependent Young's modulus and Poisson's ratio. The plastic strain is described using a plasticity model based on the Von Mises yield criterion and material properties that vary with temperature. The temperature-dependent mechanical parameters are presented in Fig. 2 [9].

Thermal strain is the strain induced by the expansion or contraction of the material due to temperature changes. Its calculation is generally based on the linear expansion coefficient of the material and the temperature variation [22], as expressed in Eq. (4):

$$\varepsilon^{th} = \alpha \bullet \Delta T \tag{4}$$

3.2 The numerical simulation model

The FEM was employed to simulate the welding experiments on butt-welded joint specimens, utilizing ABAQUS software. Temperature-dependent material properties, as shown in Fig. 2, were obtained from previous studies [23, 24]. The constitutive relations depicted in Fig. 2b, c represent true values. The thermal boundary condition accounted for heat dissipation from the model surfaces into the surrounding air. To streamline the simulation, only half of the symmetrical specimen was modeled, applying symmetric boundary conditions to the split faces. A schematic of the simulation model is provided in Fig. 3.

Conventional heat input models often utilize solid elements for simulations. In contrast, employing shell elements can reduce computational time by minimizing the number of nodal points [25, 26]. To balance model simplification with accuracy, a hybrid heat input model integrating both shell and solid elements was introduced [19]. In this model, shell elements were used in edge areas to reduce the computational time while solid elements were used in central areas to maintain the accuracy, as shown in Fig. 3. For shell elements, the

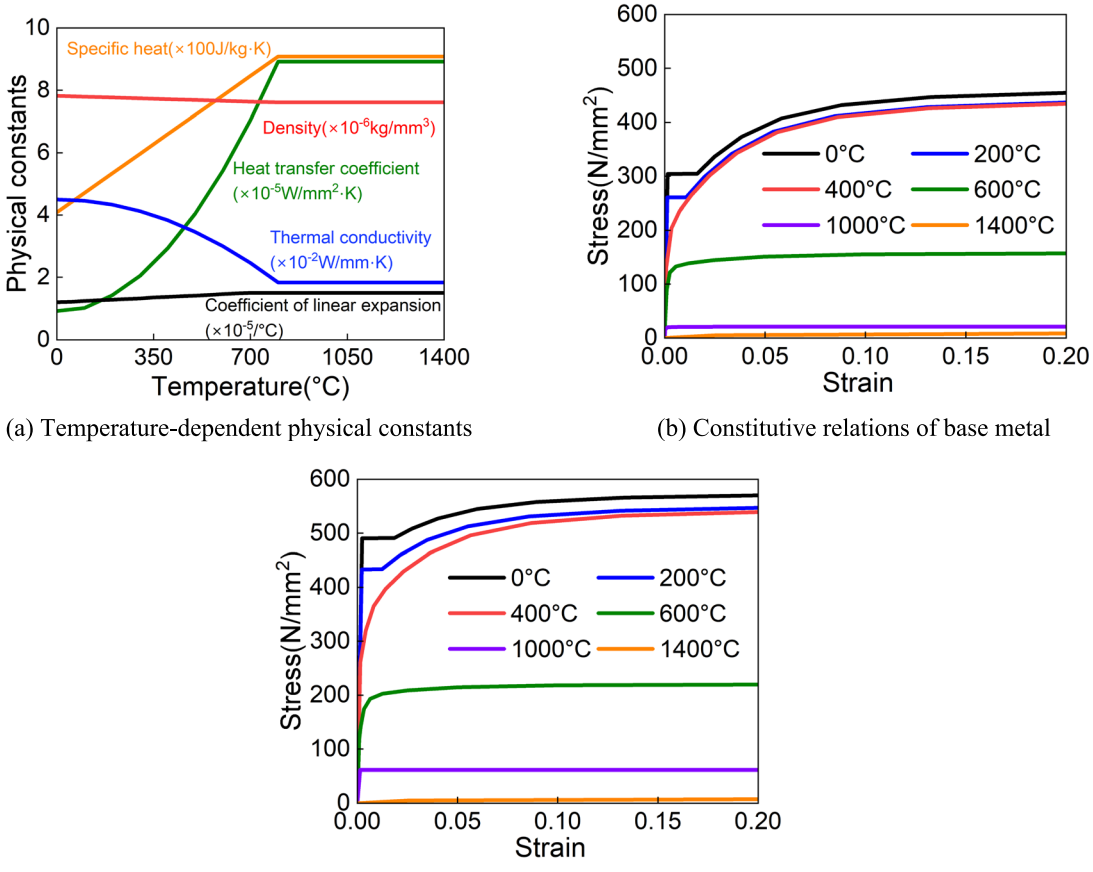

(a) Temperature-dependent physical constants

(b) Constitutive relations of base metal

(c) Constitutive relations of weld metal

Fig. 2 Temperature-dependent material properties of base metal and weld metal

Simpson rule was applied as thickness integration rule. The number of thickness integration points was five.

The combination method between the shell and solid element is shown in Fig. 3. In terms of mechanical coupling, the displacement and rotation angle of the corresponding nodal points should be consistent. The shell elements were connected to the mid-surface of the solid elements. The coupling between the shell and solid elements was achieved through a shell-solid coupling constraint. The rotation angle of the shell elements was determined by the overall displacement of the solid elements at the contact interface between the two types of elements.

In terms of thermal coupling, the shell elements employ five integration points in the thickness direction, aligning with the corresponding nodes of the solid elements. In ABAQUS, the temperature degrees of freedom (DOFs) at the integration points of the shell element, spanning from the upper surface to the lower surface, are designated as NT11 through NT15. These temperature DOFs are coupled with the temperature DOFs of the respective nodes in the solid element. This coupling ensures a consistent thermal response across the interface, thereby accurately modeling the thermal behavior of the composite structure. The integration points provide a detailed temperature distribution across the thickness of the shell element, facilitating precise thermal analysis and enhancing the fidelity of the simulation.

3.3 Heat input method

3.3.1 Discontinuous uniform heat input method

Conventional heat input models typically apply heat incrementally along the welding direction, proportionate to the size and number of meshes into which the weld bead is divided [27]. This method distributes heat uniformly across the heating area of the weld bead and is termed here as the Discontinuous Uniform (DU) heat input method for convenience. In terms of accuracy, this approach does not accurately reflect the actual heat flow characteristics by assuming uniform heat distribution within the heating area. Regarding computational efficiency, the necessity to reheat different areas and repeatedly call functions for each heat input step impacts the model's efficiency. The DU method, as applied in this model, divides the weld into 34 segments along the welding direction. This model simulates three welds in total, encompassing 105 steps: 102 heating steps and 3 cooling steps. Heat energy applied to the weld bead elements during welding was regulated by Eqs. (5) and (6). Thermal efficiency, which accounts for energy loss from the welding equipment to the plates, was determined by iteratively adjusting the model to be consistent with the measured data of temperature histories [28].

$$Q = \eta \frac{UI}{v} \tag{5}$$

$$q_m = \frac{Q}{A}\frac{v}{L} \tag{6}$$

3.3.2 Continuous distributed heat input method

To achieve a more accurate heat flux distribution and enhance the computational efficiency of welding simulations, a novel heat input method, termed the Continuous Distributed (CD) heat input method [19], is introduced.

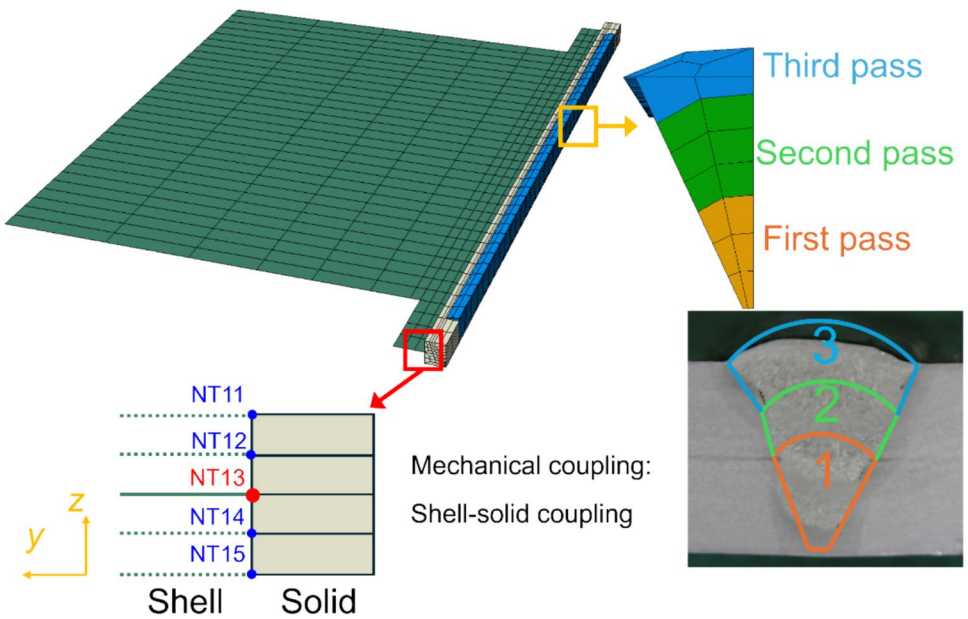

Fig. 3 Finite element model of a three-pass welded joint (symmetry model)

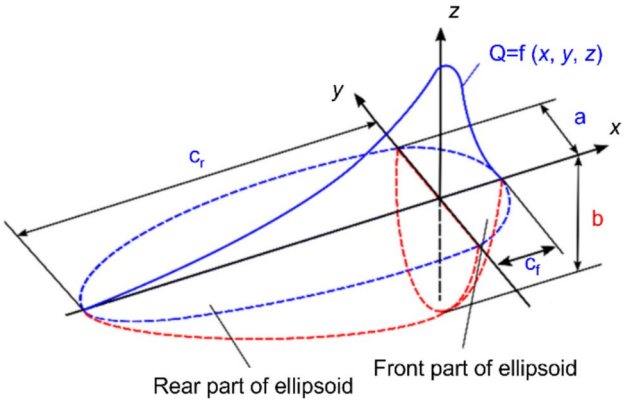

Fig. 4 Double ellipsoidal heat source model for welding simulation

This approach utilizes a double ellipsoidal heat source model to precisely replicate the actual characteristics of heat flow. The heat source model, initially proposed by Goldak [29], is mathematically represented in formulas (7), (8), and (9).

The CD method's innovative approach involves heating the entire weld bead collectively while controlling the trajectory of the heat source using a subroutine. This strategy minimizes the necessity for repeated function calls, thereby significantly boosting the model's computational efficiency. The simulation process in this model was streamlined into six steps: three dedicated to heating and three to cooling. By implementing this subroutine-based control, the CD method offered a more sophisticated and effective solution for welding simulations.

$$P = \eta UI \tag{7}$$

$$Q_f(x,y,z) = 6\sqrt{3}\frac{f_f P}{abc_f \pi\sqrt{\pi}}\exp\left(-3\left(\frac{x^2}{{c_f}^2}+\frac{y^2}{a^2}+\frac{z^2}{b^2}\right)\right) \tag{8}$$

$$Q_r(x,y,z) = 6\sqrt{3}\frac{f_r P}{abc_r \pi\sqrt{\pi}}\exp\left(-3\left(\frac{x^2}{{c_r}^2}+\frac{y^2}{a^2}+\frac{z^2}{b^2}\right)\right) \tag{9}$$

x, y, and z are point coordinates, as shown in Fig. 4.

A series of parametric analyses were conducted. Due to the large number of parameters, some parameters were approximated. f is the heat input proportion coefficient ($f_f + f_r = 2$), As practice has shown, the relation of f_f to f_r is usually accepted as a ratio of 1:2. To maintain the continuity of the introduced power, the equation $c_f : c_r = f_f : f_r$ holds. The depth of the estimated molten pool is roughly the same as the length of the front part of that ($b = c_f$) [29].

To obtain the most suitable parameters for the double ellipsoidal heat source model, it is essential to determine the estimated half-width a and half-depth b of the molten pool. These parameters were analyzed through a parametric study based on the experimentally measured actual half-width W and half-depth D of the molten pool, as shown in Table 3. The simulation results indicate that when either the ratio of a:W or b:D exceeds 1, a significant discrepancy arises between the simulation and experimental results. After comparing the simulation with the experimental results, Model A2, where the ratios of a:W and b:D converge to 0.9, showed better agreement. Figure 5 presents a comparison of the fusion zone profiles between the experimental results and the simulated results from Model A2 across three welding passes.

Table 3 Different parameters of the double ellipsoidal heat source model

Model	A1	A2	A3	A4	B1	B2	B3
a:W	0.8	0.9	1.0	1.1	0.9	0.9	0.9
b:D	0.9	0.9	0.9	0.9	0.8	1.0	1.1

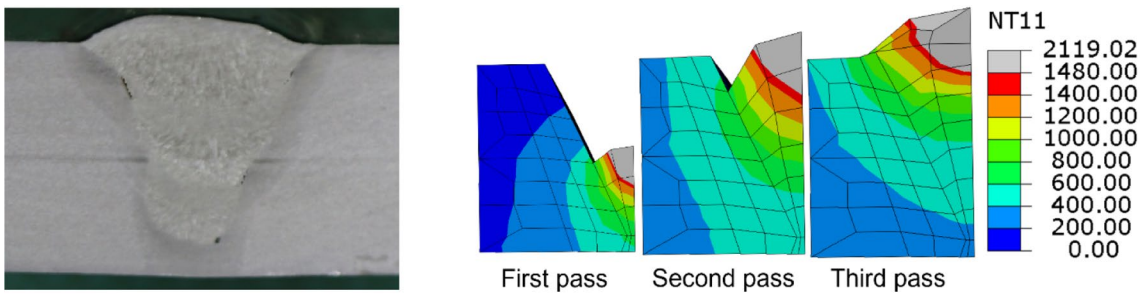

(a) Experiment (b) Simulation

Fig. 5 Fusion zone profiles in butt welding

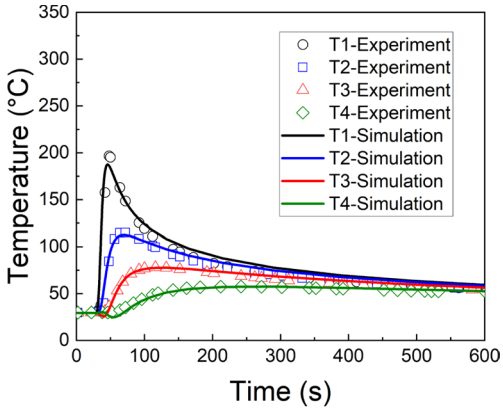

(a) First pass

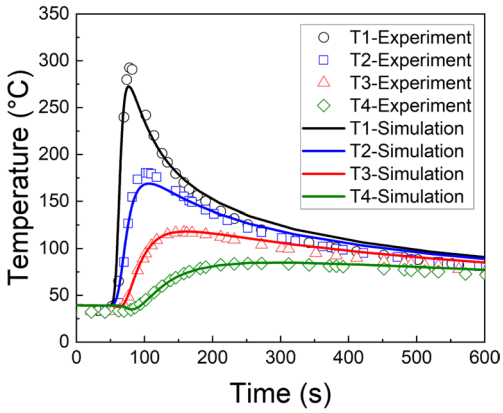

(b) Second pass

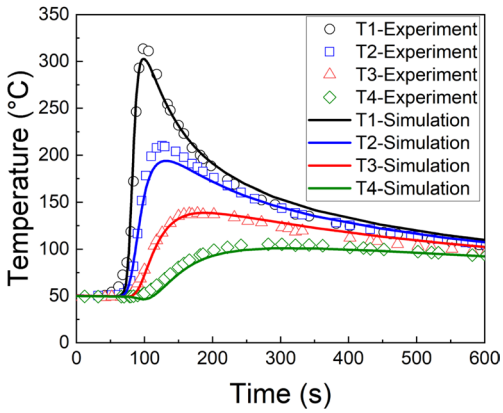

(c) Third pass

Fig. 6 Temperature histories in the welding process using the DU method

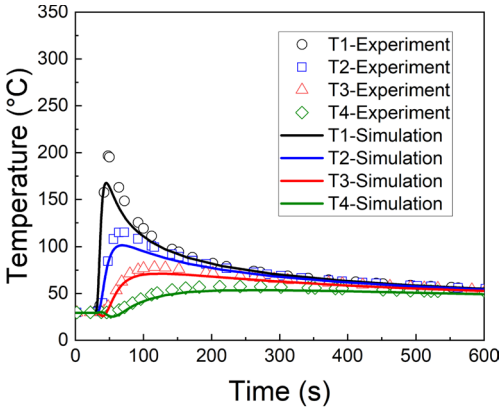

(a) First pass

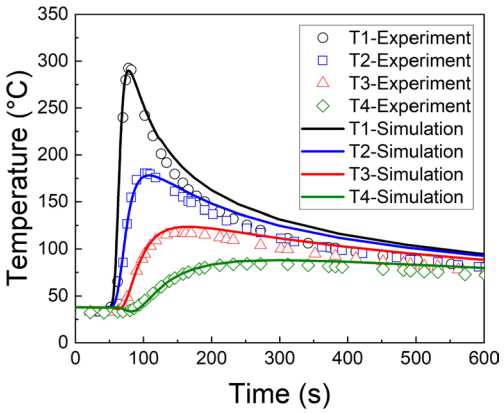

(b) Second pass

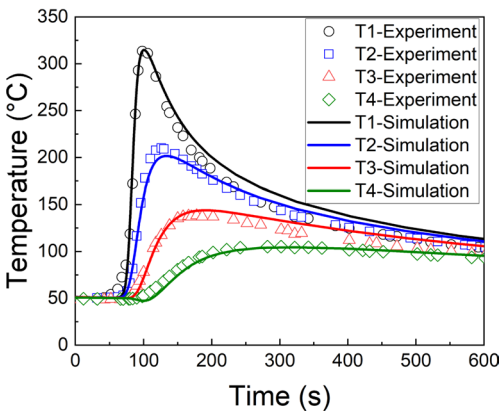

(c) Third pass

Fig. 7 Temperature histories in the welding process using the CD method

4 Experimental and analysis results

4.1 Temperature history

To assess the accuracy of simulations using two different heat input methods, the temperature variations at four thermocouple positions (T1, T2, T3, and T4) with simulation models. The temperature profiles are shown in Figs. 6 and 7.

The measurements from both samples exhibited similar trends, allowing us to use one representative sample for further analysis. Both models accurately reproduced the

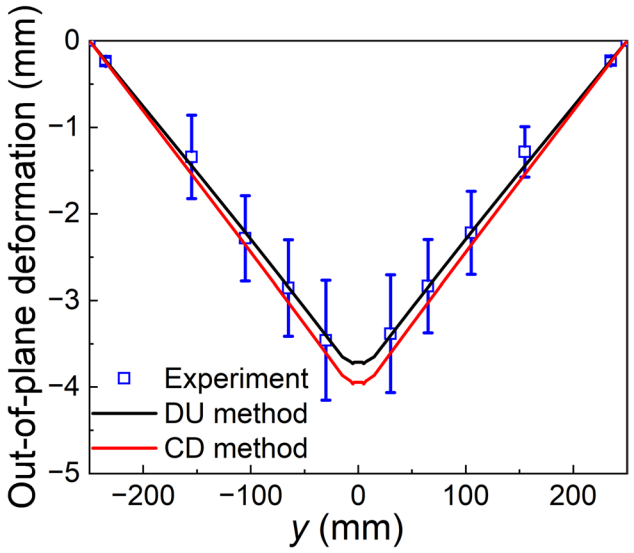

Fig. 8 Deformation comparison between experiments and simulations using the DU and CD methods

temperature variation processes at the four thermocouple positions. The thermal efficiencies of the models using the DU method and CD method were found to be 0.45 and 0.8, respectively, which fall within the typical range for arc welding. However, the thermal efficiency of 0.45 observed in the DU method is relatively low [30]. This value was determined based on the actual temperature histories recorded during the welding process. In practical welding, the heat flux distribution decreases from the center of the weld to its edges. When using the DU method, the heat input is assumed to be uniformly distributed, which tends to overestimate the heat input near the weld edges. To ensure that the simulated temperature histories align with experimental data, a lower thermal efficiency was applied. This discrepancy underscores the importance of improving the heat input method, which is one of the key focuses of this study.

Table 4 The computational time of models with different heat input methods

Heat input method	DU method	CD method
Computational time	57 min 34 s	26 min 30 s

4.2 Out-of-plane deformation

Figure 8 presents a comparison of the simulation results and experimental data regarding out-of-plane deformation. The experimental data included both the mean and standard deviation of the measurements. In the simulations, out-of-plane displacement data for nodes located along the green line in Fig. 1 were extracted to assess out-of-plane deformation. The analysis revealed that the models employing different heat input methods produce deformation patterns that are consistent with each other and align closely with the experimental results. This agreement indicates that both heat input methods demonstrate a high level of accuracy in modeling out-of-plane deformation. The similarity in the deformation trends between the simulations and experimental data underscores the reliability of the models and the effectiveness of the different heat input approaches in accurately capturing the deformation behavior.

4.3 Residual stress

Figure 9 illustrates the residual stresses in both the welding direction (x) and its orthogonal direction (y), as measured along the orange line depicted in Fig. 1. The experimental

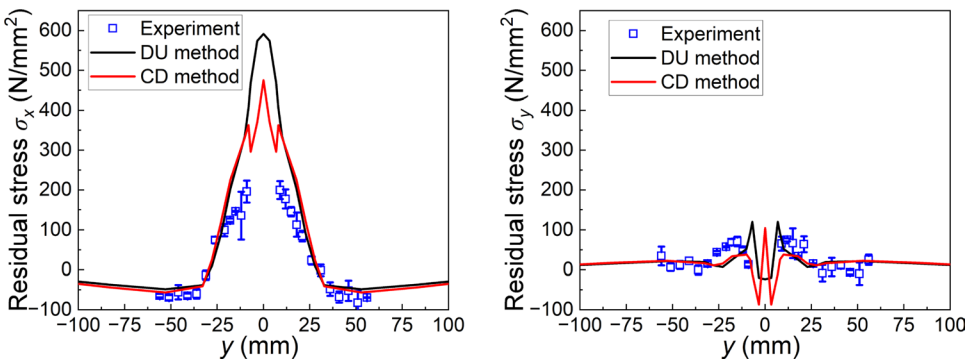

(a) In the x direction

(b) In the y direction

Fig. 9 Residual stresses comparison between experiments and simulations using the DU and CD methods

data presented include both the mean values and the standard deviations of the measured stress components, providing a comprehensive overview of the residual stress distribution. In the simulation, stress values were extracted for nodes along the orange line in Fig. 1. These simulated stress values were compared with the experimental data, and the results demonstrate that the analytical models, irrespective of the heat input method used, closely align with the overall trends observed in the experimental data. This consistency highlights the accuracy of the models in predicting residual stress distributions, particularly in the base metal regions adjacent to the weld zone.

However, the two methods show different peak values of residual stress in the central weld zone. Due to the inherent limitations of X-ray diffraction (XRD), this method is not applicable for accurately measuring residual stresses within the weld zone, because of the complex microstructure in this region. This limitation makes it more difficult to validate the predicted stress state in the weld zone. This study primarily focuses on the residual stress distribution trends in the base metal regions adjacent to the weld zone. Future work will aim to further investigate and refine the simulation models to improve accuracy in predicting the stress state within the weld zone itself.

4.4 Computational time

To provide a more accurate comparison of the computational efficiency of models employing different heat input methods, all simulations were performed on the same computer, equipped with a 2.50 GHz CPU and 8 cores. Table 4 summarizes the computational times for both models: the DU heat input model required 57 min and 34 s, while the CD heat input model completed the analysis in 26 min and 30 s. These results clearly demonstrate that the CD method significantly reduces computational time compared to the DU method, without compromising accuracy. This finding highlights the superior efficiency of the CD heat input model, making it a more practical choice for scenarios where balancing computational resources and accuracy is crucial. In the current simulations, due to the relatively small size of the components, the computational time for both methods is relatively short. However, for larger or more detailed components, the time-saving advantage of the CD method will become more pronounced.

5 Conclusions

In this investigation, an integrated approach combining experimental investigations and numerical simulations was employed to develop an optimized FEM tailored for the simulation of the three-pass butt welding process. The principal discoveries are delineated as follows:

(1) To streamline the simulation model and reduce its intricacies, a hybridization of shell and solid elements was adopted. This methodological fusion led to a substantial reduction in the size of the stiffness matrix, thereby improving computational efficiency. The comparative analysis between simulation results and experimental data demonstrated a high degree of concordance, underscoring the model's adeptness at forecasting butt welding deformation and residual stresses.

(2) A novel heat input method, termed the Continuous Distributed (CD) method, was introduced to curtail computational time. This approach accommodates the continuous movement and double ellipsoidal distribution of energy. By leveraging the CD method, the model's complexity was diminished, and energy distribution efficiency markedly improved. The CD method's application resulted in a reduction of computational time to just 46% of that required by the conventional Discontinuous Uniform (DU) heat input method.

The implementation of a simulation model integrating the CD method alongside shell and solid elements effectively streamlined the modeling process and minimized computation time. Nonetheless, given that the model was limited to a three-pass welding scenario, its broader applicability remains somewhat restricted, and its generalizability has yet to be thoroughly assessed. In cases involving multi-pass welding, it is crucial to evaluate the impact of weld bead configurations on simulation results. Future research will encompass multi-pass welding experiments to validate the model's adaptability across various welding conditions.

This research primarily aimed to augment computational efficiency while preserving the accuracy of the simulation model. Subsequent investigations will focus on exploring the extended applicability of the proposed heat input method across a wider range of welding scenarios.

Appendix

Table 5

Table 5 List of symbols and their definitions

Symbol/abbreviation	Definition	Unit
T	Temperature	K
$\mathcal{H}$	Enthalpy (per unit volume)	J/mm^3
κ	The material thermal conductivity	W/mm·K
q	The welding volume heat input	W/mm^3
ρ	Density of the material	kg/mm^3
Ω_i	Spatial domain where the equation is applied	–
$(\boldsymbol{x}, t)$	Spatial and temporal coordinates	mm, s
$\dot{\boldsymbol{\epsilon}}$	Total strain rate	s^{-1}
$\dot{\boldsymbol{\epsilon}}^{\mathrm{e}}$	Elastic strain rate	s^{-1}
$\dot{\boldsymbol{\epsilon}}^{\mathrm{p}}$	Plastic strain rate	s^{-1}
$\dot{\boldsymbol{\epsilon}}^{\mathrm{th}}$	Thermal strain rate	s^{-1}
$\widehat{\boldsymbol{\sigma}}_{\mathrm{GN}}$	Objective stress rate	Pa/s
$\boldsymbol{E}^{\mathrm{e}}$	Matrix with the elastic material properties	Pa
$\dot{T}$	Rate of temperature change	K/s
α	Linear thermal expansion coefficient	K^{-1}
ΔT	Change in temperature	K
Q	Welding heat energy	J/mm
η	Thermal efficiency	–
U	Voltage of the welding equipment	V
I	Current for the welding	A
v	Welding speed	mm/s
A	Cross-sectional area of the heat input elements	mm^2
L	Length of the heat input elements	mm
q_m	Welding heat energy per unit volume	J/mm^3
P	Total introduced power	W
Q_f	Volumetric heat flux density in front part of the model	W/mm^3
Q_r	Volumetric heat flux density in rear part of the model	W/mm^3
a	Half-width of the estimated molten pool	mm
b	Half-depth of the estimated molten pool	mm
c_f	Length of the front part of the estimated molten pool	mm
c_r	Length of the rear part of the estimated molten pool	mm
f_f	Forward heat fraction	–
f_r	Rearward heat fraction	–
W	Half-width of the actual molten pool	mm
D	Half-depth of the actual molten pool	mm

Author contribution All authors contributed to the study conception and design. Experimental data analysis, numerical simulation modeling, and manuscript drafting were performed by Xiaoyu Guan. Mikihito Hirohata provided experimental equipment, materials, and made critical revisions and annotations to the manuscript. Kyong-Ho Chang made critical revisions and annotations to the manuscript. All authors read and approved the final manuscript.

Funding Open Access funding provided by Osaka University.

Data availability The datasets generated and/or analyzed during the current study are not publicly available due to the proprietary nature of the data but are available from the corresponding author upon reasonable request.

Declarations

Competing interests The authors declare no competing interests.

References

1. Deng D, Liang W, Murakawa H (2007) Determination of welding deformation in fillet-welded joint by means of numerical simulation and comparison with experimental measurements. J Mater Process Technol 183(2–3):219–225
2. Teng TL, Chang PH, Tseng WC (2003) Effect of welding sequences on residual stresses. Comput Struct 81(5):273–286
3. Hirohata M, Chang KH, Suzuki T, Konishi H (2024) Local heating for reducing residual stress and fatigue-performance improvement of welded joints. J Constr Steel Res 215:108544
4. Michaleris P, DeBiccari A (1997) Prediction of welding distortion. Welding Journal-Including Welding Research Supplement 76:172–181
5. Gannon L, Liu Y, Pegg N, Smith MJ (2012) Effect of welding induced residual stress and distortion on ship hull girder ultimate strength. Mar Struct 28:25–49
6. Krebs J, Kassner M (2007) Influence of welding residual stresses on fatigue design of welded joints and components. Weld World 51(7–8):54–68
7. Wikander L, Karlsson L, Nasstrom M et al (1994) Finite element simulation and measurement of welding residual stresses. Modell Simul Mater Sci Eng 2(4):845
8. Takechi S, Aoyama K, Nomoto T (1998) Basic studies on accuracy management systems based on estimating welding deformations. J Mar Sci Technol 3:194–200
9. Deng D, Murakawa H, Liang W (2007) Numerical simulation of welding distortion in large structures. Comput Methods Appl Mech Eng 196(45–48):4613–4627
10. Liu Y, Wang P, Fang H et al (2021) Mitigation of residual stress and deformation induced by TIG welding in thin-walled pipes through external constraint. J Market Res 15:4636–4651
11. Zhang C, Sun J, Li Y et al (2022) Numerical simulation of residual stress of butt-welded joint involved in complex column-beam welded structure. J Manuf Process 83:458–470
12. Das D, Bag S, Pal S (2024) A physics-informed machine learning model of dissimilar friction stir welding to tailor residual stress using coupled Eulerian and Lagrangian approach. J Mater Eng Perform 1–9
13. De A, DebRoy T (2011) A perspective on residual stresses in welding. Sci Technol Weld Joining 16(3):204–208
14. Mahmood MA, Tariq U, Oane M, Liou F (2024) Analytical and FEM models for thermal analysis and residual stresses using wire arc-based welding and additive manufacturing of SUS304. Int J Adv Manuf Technol 1–18
15. Huang H, Ma N, Rashed S, Narasaki K, Kado K, Agano Y, Mao W (2024) Experimental and numerical investigation of a gouging heat source model and gouging/welding residual stress and deformation. J Manuf Process 110:101–113
16. Murakawa H, Ma N, Huang H (2015) Iterative substructure method employing concept of inherent strain for large-scale welding problems. Welding in the World 59:53–63
17. Ikushima K, Shibahara M (2014) Prediction of residual stresses in multi-pass welded joint using idealized explicit FEM accelerated by a GPU. Comput Mater Sci 93:62–67
18. Hirohata M, Nozawa S, Tokumaru Y (2022) Verification of FEM simulation by using shell elements for fillet welding process. Int J Interact Des Manuf 16(4):1601–1613
19. Guan X, Hirohata M (2024) Effective FE simulation methods for fillet welding process by continuous distributed heat input and element combination. Finite Elem Anal Des 236:104181
20. Hirohata M, Itoh Y (2016) A simplified FE simulation method with shell element for welding deformation and residual stress generated by multi-pass butt welding. Int J Steel Struct 16:51–58
21. Anca A, Cardona A, Risso J, Fachinotti VD (2011) Finite element modeling of welding processes. Appl Math Model 35(2):688–707
22. Wu C, Wang C, Kim JW (2021) Welding distortion prediction for multi-seam welded pipe structures using equivalent thermal strain method. J Weld Join 39(4):435–444
23. Hanji T, Tateishi K, Kano S et al (2020) Fatigue strength of transverse attachment steel joints with single-sided arc weld using low transformation temperature welding consumable. Weld World 64:1293–1301
24. Aung MP, Katsuda H, Hirohata M (2019) Fatigue-performance improvement of patch-plate welding via PWHT with induction heating. J Constr Steel Res 160:280–288
25. Zhang YM, Kovacevic R, Li L (1996) Characterization and real-time measurement of geometrical appearance of the weld pool. Int J Mach Tools Manuf 36(7):799–816
26. Wang X, Li R (2014) Intelligent modelling of back-side weld bead geometry using weld pool surface characteristic parameters. J Intell Manuf 25:1301–1313
27. Jiang WC, Wang BY, Gong JM et al (2011) Finite element analysis of the effect of welding heat input and layer number on residual stress in repair welds for a stainless steel clad plate. Mater Des 32(5):2851–2857
28. Dupont JN, Marder AR (1995) Thermal efficiency of arc welding processes. Welding Journal-Including Welding Research Supplement 74(12):406s
29. Goldak J, Chakravarti A, Bibby M (1984) A new finite element model for welding heat sources. Metall Trans B 15:299–305
30. Michaleris P, DeBiccari A (1997) Prediction of welding distortion. Weld J 76(4):172s